A novel mathematical model for the effects of wall properties on pumping flow of a biofluid in a symmetrical three-dimensional curved duct

Wafa F. Alfwzan[1], Arshad Riaz[2]*, Maha Alammari[3], Hala A. Hejazi[4] and ElSayed M. Tag El-Din[5]

[1]Department of Mathematical Sciences, College of Science, Princess Nourah bint Abdulrahman University, Riyadh, Saudi Arabia, [2]Department of Mathematics, Division of Science and Technology, University of Education Lahore, Lahore, Pakistan, [3]Department of Mathematics, College of Science, King Saud University, Al-Riyadh, Saudi Arabia, [4]Mathematical Sciences Department, College of Applied Sciences, Umm Al-Qura University, Makkah, Saudi Arabia, [5]Center of Research, Faculty of Engineering, Future University in Egypt, New Cairo, Egypt

Most pumping actions entail a physical volume change of the duct, which is frequently achieved by having a compliant wall or membrane. To the best of our knowledge, the current study is the first report on a mathematical model developed to analyze the peristaltic transport of a Newtonian fluid in a curved duct with rectangular face and compliant walls. Such geometries are most commonly used in clinical and biological equipment, where the walls of the duct need to be flexible. Flexible ducts are more useful than rigid ones because they do not require any extra modifications or accessories. Here, we have used the conditions of lubrication theory to construct an accurate model, and a common perturbation technique was incorporated to handle the Navier-Stokes equations with emphasis on various aspect ratios and curvatures. A system of curvilinear coordinates operating according to the principles of the cylindrical system was employed to represent the mathematical problem. No-slip boundary limitations were considered at the walls along with the extra constraint of compliant walls showing damping force and stiffness. Comprehensive graphical representations were made to illustrate the effects of all emerging factors of the study in both two- and three-dimensional formats. We found that large curvatures and flexure rigidity decreased the fluid velocity uniformly, but the aspect ratio and amplitude parameters could promote fluid velocity. Validation of the results was performed through the generation of a residual error curve. The current readings were taken again with a straight duct to make a comparison with the existing literature.

KEYWORDS

duct of the curved axis, wavy flow, elastic walls, no-slip conditions, Newtonian liquid, HPM, curvilinear/cylindrical system

1 Introduction

Peristalsis describes the mechanism whereby rhythmic contraction and expansion of the walls of tubing propels the contents forward. Physiologically, peristalsis is the primary motive force in all flow processes in the human body including the passage of food from the mouth to the esophagus, urine flow from the kidney through the bladder, blood flow in the arteries, and sperm passage through the urethra. Because of the versatility and efficiency of peristaltic flow, many researchers are currently working on applications of this type of fluid transport. Javed and Naz [1] have determined the pumping stream characteristics of Jeffrey model material in a wavy, asymmetric compliant channel by taking very small amplitudes and discovered that peristaltic reversal of the flow occurred at the boundaries. Khan et al. [2] studied the magnetohydrodynamic transport of a nanofluid composed of particles of different shapes in a channel with peristaltic walls, and they found that the heat generated could produce large temperature increases in the fluid. Raza et al. [3] published a numerical and analytical study of the effects of an induced magnetic field on the wavy features of various CNTs through an asymmetric porous channel, and pressure gradient curves showed a reduction in height with large values of the heat generation factor. A study by Imran et al. [4] addressed the components of a homogeneous–heterogeneous reaction on the peristaltic motion of a Rabinowitsch flow model in a flexible channel. They employed a lubrication approach for the analysis and found that the considered reaction exhibited a reversal of the concentration field. Hayat et al. [5] considered the flow characteristics of a Sutterby fluid model in an orthogonal peristaltic channel with thermal exchange and compliant walls and determined that the fluid reacted with higher velocity and temperature diffusion in contrast to the viscous liquid. However, all such studies were conducted in two-dimensional channels, and more results with this type of model are reported in [6–12].

Most of the geometries used in medical equipment like endoscopes and catheters involve curved shapes. Duct configuration is also very important in the design of industrial equipment to exhaust dust particles. Rashid et al. [13] investigated the influence of magnetic fields on a Williamson model in a curved enclosure with peristaltic activity and noted that the strength of the generated magnetic field was reduced for a Williamson liquid compared to a Newtonian fluid. Anber et al. [14] reported the results of a study of the pumping characteristics of a hybrid nanofluid in a curved enclosure, while Riaz et al. [15] discussed the thermal characteristics of nanoparticles distributed in a curved channel. They assumed that the slip constraint of the walls was of the second order and concluded that slip parameters can produce opposite readings with respect to the flow attributes throughout the domain. Ahmed et al. [16] obtained numerical results for peristaltic flow and mixed convection phenomena across a curved geometry and concluded that flow properties such as fluid speed were greater as a result of large thermal Grashof and Hartmann numbers. In their work, Hina et al. [17] performed a heat and mass analysis for peristaltic transport of a Johnson–Segalman model in a flexible curved conduit and concluded from their observations that the axial velocity of a non-linear liquid was higher than that of a viscous material.

Most fluid flows in the human body and in medical instrumentation are directly influenced by the 3-D structure. Keeping in mind the core applications of blood flow in arteries and the pumping mechanism of a peristaltic pump, researchers have found it necessary to investigate the nature of three-dimensional peristaltic streams. Ellahi et al. [18] have contributed to the literature in their study of wavy pumping in a non-uniform rectangular 3-D duct enclosure by performing a heat-mass exchange analysis. They generated some exact solutions to the problem and also discussed the limiting cases of the duct. Mekheimer et al. [19] tested the effect of wall flexibility on the wavy stream in an asymmetric duct of rectangular shape and concluded that the pressure gradient was higher in the duct than in a channel of any geometry. Akram and Saleem [20] focused on the thermal phenomena associated with various forms of complex waves for the peristaltic motion of a Carreau model in ducts of various geometries and claimed that the number of trapping circulation contours was decreased by the large aspect ratio of the conduit. Saleem et al. [21] assumed the peristaltic heated flow of a non-linear fluid in an elliptical duct and concluded that the elliptical duct was preferable in some industrial systems over a circular type of enclosure. Akbar and Butt [22] considered a nanofluid model undergoing peristaltic transport in a plumb duct and summed up their investigation with the conclusion that when pure water was transferred to a Cu-water, trapped boluses at the upper side became larger but were fewer in number. Curved configurations are frequently used in real hydraulic structures as curved diffusers in hydraulic turbines, S-shaped bulb turbines, and fittings, etc. [23]. Li et al. [24] executed an experimental and quantitative comparison to understand the features of three-dimensional flows in a 120° curved duct with a rectangular face and varying curvature, which is the design most often used for two-phase centrifugal pumps. They tested three different curvatures, the double circular line, the spiral line, and the involute line, and also assumed three aspect ratios of 0.4, 1.0, and 2.3 with very large Reynolds numbers. On the basis of their numerical data and experimental readings, they concluded that the flow characteristics in a duct with continuously varying curvature were very different from those of a constant curvature duct. Ghia and Sokhey [25] examined the incompressible laminar transport of a viscous fluid in a rectangular-faced curved duct and formulated a model with three-dimensional parabolized governing equations by taking two forms of the coordinate system; they fully discussed the effects of longitudinal curvature on flow attributes. Recently, Dolon et al. [26] performed a computational analysis of general flow and heat transport through a curved rectangular duct and revealed that the flow characteristics were highly affected by the curved shape and the aspect ratio. They also declared that the thermal exchange capacity of the fluid was enhanced in the curved duct. Recently, Riaz et al. [27] published their work on peristaltic flow in a curved rectangular duct and concluded that the pumping rate was lower in ducts with large curvature and aspect ratios. Further information on 3-D flows can be found in [28, 29].

In our survey of the peristaltic pump literature, we found no studies that discuss the peristaltic flow characteristics of a viscous fluid in a curved duct of rectangular cross-section with compliant walls. Thus, keeping in mind the remarkable success in biological and mechanical systems of the application of compliant walls on pumping flows in curved ducts, the authors sought to produce some
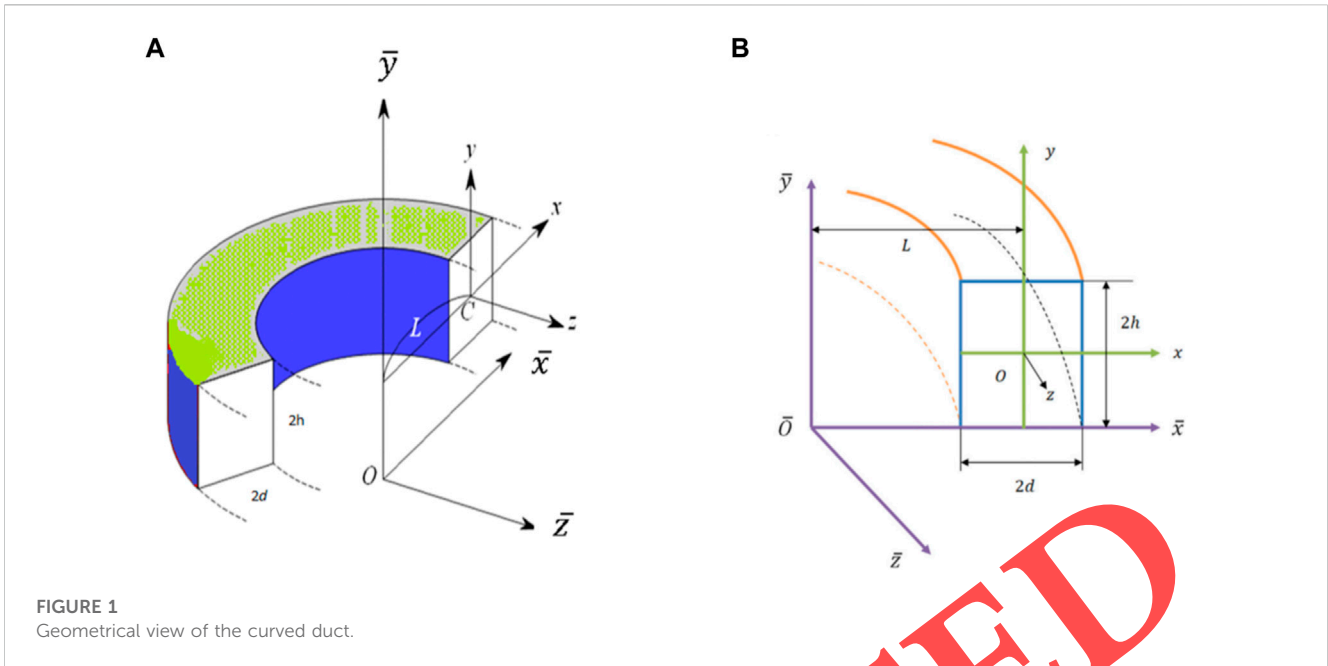
FIGURE 1
Geometrical view of the curved duct.

mathematical representations of the peristaltic flow of a viscous fluid in a curved duct of rectangular cross-section having compliant surfaces. These results should be helpful in many industrial and medical systems where curved geometries are preferred to straight ones as discussed previously. A three-dimensional cylindrical coordinate system was used here initially and later converted into a curvilinear system by introducing suitable transformations. Based on lubrication theory, the mathematical features of the problem have been expressed as a set of partial differential equations with variable coefficients, which can be handled by a common perturbation strategy. A system of compliant walls, which expressed the pressure gradient at the boundaries, was assumed together with the no-slip boundary conditions. In the last part of the study, the results obtained analytically were plotted as velocity fields (both 2-D and 3-D) with streamlines to examine the core effects of various emerging parameters on the flow properties. Axial velocity was also plotted against the curvature coordinates to estimate the direct impact of curvature on the different flow regimens.

2 Mathematical modeling

Considering a fluid under conditions of a linear stress–strain model flowing through a curved rectangular duct (CRD) of height, $2h$, and width, $2d$, a sinusoidal wave with uniform speed, c, was generated along a longitudinal path. The arrangement of the conduit assumed that the elastic walls produced waves along the vertical axis (y-axis), whose equations have been taken through a function of angle θ and time t. L is the reference length from central point O, as shown in Figure 1, while the flow structure was managed as a cylindrical frame of reference, with r, θ and y assumed as the reference variables.

The equations for the conservation of mass and momentum in the cylindrical system for the velocity field (u, w, v) are expressed as in [26]:

$$\frac{\partial u}{\partial r} + \frac{1}{r}\frac{\partial w}{\partial \theta} + \frac{\partial v}{\partial y} + \frac{u}{r} = 0 \tag{1}$$

$$\frac{\partial u}{\partial t} + (V \cdot \mathrm{E})u - \frac{w^2}{r} = -\frac{1}{\rho}\frac{\partial p}{\partial r} + \frac{\mu}{\rho}\left(\Delta^\star u - \frac{u}{r^2} - \frac{2}{r^2}\frac{\partial w}{\partial \theta}\right) \tag{2}$$

$$\frac{\partial w}{\partial t} + (V \cdot \mathrm{E})w \mp \frac{uw}{r} = -\frac{1}{\rho r}\frac{\partial p}{\partial \theta} + \frac{\mu}{\rho}\left(\Delta^\star w - \frac{w}{r^2} + \frac{2}{r^2}\frac{\partial u}{\partial \theta}\right) \tag{3}$$

$$\frac{\partial v}{\partial t} + (V \cdot \mathrm{E})v = -\frac{1}{\rho}\frac{\partial p}{\partial y} + \frac{\mu}{\rho}\left(\Delta^\star v\right). \tag{4}$$

Here, $V \cdot \mathrm{E}$ and $\Delta^\star$ are first- and second-order differential operators, correspondingly, which are defined as $V \cdot \mathrm{E} = u\frac{\partial}{\partial r} + \frac{w}{r}\frac{\partial}{\partial \theta} + v\frac{\partial}{\partial y}$, $\Delta^\star = \frac{\partial^2}{\partial r^2} + \frac{1}{r}\frac{\partial}{\partial r} + \frac{1}{r^2}\frac{\partial^2}{\partial \theta^2} + \frac{\partial^2}{\partial y^2}$.

The peristaltic walls are represented by

$$\tilde{a}(\theta, t) = h + b\cos\frac{2\pi}{\lambda}(L\theta - ct) \tag{5}$$

where b is the wave amplitude and λ is the wavelength. The aforementioned equations were non-dimensionalized by the application of the following transformations [26, 27]:

$$\bar{t} = \frac{c}{\lambda}t, \bar{u} = \frac{1}{c\xi}u, \bar{v} = \frac{1}{c\xi}v, \bar{w} = \frac{1}{c}w, r = L + d\bar{x}, y = h\bar{y}, a = \frac{\tilde{a}}{h}, L\theta$$

$$= \lambda\bar{z}, \bar{p} = \frac{d^2}{c\lambda\mu}p \tag{6}$$

Here, $\xi\ (= \frac{h}{\lambda})$ is the wave number, μ is the fluid viscosity, t gives the time, and p is the pressure. By utilizing the relation (6), Eqs 1–5 are transformed to

$$\alpha\frac{\partial \bar{u}}{\partial \bar{x}} + \frac{1}{1 + \delta\bar{x}}\frac{\partial \bar{w}}{\partial \bar{z}} + \frac{\partial \bar{v}}{\partial \bar{y}} + \frac{\alpha\delta}{1 + \delta\bar{x}}\bar{u} = 0 \tag{7}$$

$$Re\,\xi\alpha\left(\xi^2\frac{\partial\bar{u}}{\partial\bar{t}} + \alpha\xi^2\bar{u}\frac{\partial\bar{u}}{\partial\bar{x}} + \xi^2\bar{v}\frac{\partial\bar{u}}{\partial\bar{y}} + \frac{\xi^2\bar{w}}{1+\delta\bar{x}}\frac{\partial\bar{u}}{\partial\bar{z}} - \frac{\alpha\delta}{1+\delta\bar{x}}\bar{w}^2\right)$$

$$= \xi^2\left(\alpha^2\frac{\partial^2\bar{u}}{\partial\bar{x}^2} + \frac{\delta\alpha^2}{1+\delta\bar{x}}\frac{\partial\bar{u}}{\partial\bar{x}} + \frac{\xi^2}{(1+\delta\bar{x})^2}\frac{\partial^2\bar{u}}{\partial\bar{z}^2} + \frac{\partial^2\bar{u}}{\partial\bar{y}^2} - \left(\frac{\alpha\delta}{1+\delta\bar{x}}\right)^2\bar{u}\right)$$

$$-2\alpha\left(\frac{\delta^{1/2}}{1+\delta\bar{x}}\right)^2\frac{\partial\bar{w}}{\partial\bar{z}} - \alpha^3\frac{\partial\bar{p}}{\partial\bar{x}} \quad (8)$$

$$Re\,\xi\left(\alpha\frac{\partial\bar{w}}{\partial\bar{t}} + \alpha^2\bar{u}\frac{\partial\bar{w}}{\partial\bar{x}} + \alpha\bar{v}\frac{\partial\bar{w}}{\partial\bar{y}} + \frac{\alpha\bar{w}}{(1+\delta\bar{x})}\frac{\partial\bar{w}}{\partial\bar{z}} - \frac{\alpha^2\delta}{(1+\delta\bar{x})}\bar{u}\bar{w}\right)$$

$$= \left(\alpha^2\frac{\partial^2\bar{w}}{\partial\bar{x}^2} + \frac{\delta\alpha^2}{1+\delta\bar{x}}\frac{\partial\bar{w}}{\partial\bar{x}} + \frac{\xi^2}{(1+\delta\bar{x})^2}\frac{\partial^2\bar{w}}{\partial\bar{z}^2} + \frac{\partial^2\bar{w}}{\partial\bar{y}^2} - \left(\frac{\alpha\delta}{1+\delta\bar{x}}\right)^2\bar{w}\right)$$

$$+2\alpha\xi^2\left(\frac{\delta^{1/2}}{1+\delta\bar{x}}\right)^2\frac{\partial\bar{u}}{\partial\bar{z}} - \frac{\alpha^2}{1+\delta\bar{x}}\frac{\partial\bar{p}}{\partial\bar{z}} \quad (9)$$

$$Re\,\xi^3\left(\frac{1}{\alpha}\frac{\partial\bar{v}}{\partial\bar{t}} + \bar{u}\frac{\partial\bar{v}}{\partial\bar{x}} + \frac{1}{\alpha}\bar{v}\frac{\partial\bar{v}}{\partial\bar{y}} + \frac{\bar{w}}{\alpha(1+\delta\bar{x})}\frac{\partial\bar{v}}{\partial\bar{z}}\right)$$

$$= \xi^2\left(\frac{\partial^2\bar{v}}{\partial\bar{x}^2} + \frac{\delta}{1+\delta\bar{x}}\frac{\partial\bar{v}}{\partial\bar{x}} + \frac{\xi^2}{\alpha^2(1+\delta\bar{x})^2}\frac{\partial^2\bar{v}}{\partial\bar{z}^2} + \frac{1}{\alpha^2}\frac{\partial^2\bar{v}}{\partial\bar{y}^2}\right) - \frac{\partial\bar{p}}{\partial\bar{y}}. \quad (10)$$

In the aforementioned relations, the new dimensionless quantities produced are described as follows:

$$\alpha = \frac{h}{d}, \delta = \frac{d}{L}, Re = \frac{\rho d c}{\mu}, \xi = \frac{h}{\lambda}, \phi = \frac{b}{h}. \quad (11)$$

Using criteria of long wavelength and smallest Reynolds' number provides the reduced form of Eqs 8–10, which is shown as follows (exempting the bars):

$$\frac{\partial p}{\partial x} = 0, \quad (12)$$

$$\frac{\alpha^2}{1+\delta x}\frac{\partial p}{\partial z} = \alpha^2\frac{\partial^2 w}{\partial x^2} + \frac{\delta\alpha^2}{1+\delta x}\frac{\partial w}{\partial x} + \frac{\partial^2 w}{\partial y^2} - \left(\frac{\alpha\delta}{1+\delta x}\right)^2 w, \quad (13)$$

$$\frac{\partial p}{\partial y} = 0. \quad (14)$$

Eqs 12–14 predict that $\bar{p}\neq\bar{p}(\bar{x},\bar{y})$, and from Eq. 13, we get the final equation (after dropping the bars) to be solved as described as follows:

$$\frac{\alpha^2}{1+\delta x}\frac{\partial p}{\partial z} = \alpha^2\frac{\partial^2 w}{\partial x^2} + \frac{\delta\alpha^2}{1+\delta x}\frac{\partial w}{\partial x} + \frac{\partial^2 w}{\partial y^2} - \left(\frac{\alpha\delta}{1+\delta x}\right)^2 w. \quad (15)$$

The relevant boundary function values for the flow mechanism are suggested as follows:

$$w(\bar{x}, \pm\bar{a}) = 0 \text{ and } w(\pm d, \bar{y}) = 0 \quad (16)$$

where peristaltic walls are considered as compliant, resulting in an equation whose basic form is as follows [17]:

$$\left(-\tau\frac{\partial^3}{\partial z^3} + \sigma\frac{\partial^3}{\partial z\partial t^2} + \varepsilon\frac{\partial^2}{\partial z\partial t}\right)\tilde{a} = \frac{\partial p}{\partial z}, at\ y = \pm\tilde{a}, \quad (17)$$

where $\tau, \sigma,$ and ε reflect the elastic membrane tension, mass over the unit area, and viscous damping coefficient, respectively. In dimensionless fashion (with no bar signs), Eqs 13 and 14 take the form of

$$w(x, \pm a) = 0 \text{ and } w(\pm 1, y) = 0, \text{where } a = 1 + \phi\cos 2\pi(z-t) \quad (18)$$

$$\left(E_1\frac{\partial^3}{\partial z^3} + E_2\frac{\partial^3}{\partial z\partial t^2} + E_3\frac{\partial^2}{\partial z\partial t}\right)\tilde{a} = \frac{\partial p}{\partial z}, at\ y = \pm a \quad (19)$$

3 Solution scheme

In order to solve the PDE obtained in Eq. 15 along with the B.Cs displayed in Eqs 18 and 19, a well-known perturbation technique (HPM) [30–32] was employed. The linear operator chosen in the process was $\Psi_{yy} = \partial^2/\partial y^2$. The initial guess for satisfying the conditions was $w_0 = \frac{\pi(z)(-a^2+y^2)\alpha^2}{2+2x\delta}$. The zeroth and first-order systems have the following respective forms:

$$\Psi_{yy}\hat{w}_0 - \Psi_{yy}w_0 = 0, \hat{w}_0(x, \pm a) = 0 \text{ and } \hat{w}_0(\pm 1, y) = 0 \quad (20)$$

$$\Psi_{yy}\hat{w}_1 + \Psi_{yy}\hat{w}_0 + \alpha^2\Psi_{xx}\hat{w}_0 + \frac{\delta\alpha^2}{1+\delta x}\Psi_x\hat{w}_0 - \left(\frac{\alpha\delta}{1+\delta x}\right)^2 w - \frac{\alpha^2}{1+\delta x}\pi(z) = 0,$$

$$\hat{w}_1(x, \pm a) = 0 \text{ and } \hat{w}_1(\pm 1, y) = 0 \quad (21)$$

$$\Psi_{yy}\hat{w}_2 + \alpha^2\Psi_{xx}\hat{w}_1 + \frac{\delta\alpha^2}{1+\delta x}\Psi_x\hat{w}_1 - \left(\frac{\alpha\delta}{1+\delta x}\right)^2 w_1 = 0, \hat{w}_2(x, \pm a)$$

$$= 0 \text{ and } \hat{w}_2(\pm 1, y) = 0 \quad (22)$$

By solving the aforementioned three systems simultaneously using the built-in command, DSolve of Mathematica, we generated the solutions of axial velocity parts $w_0, w_1,$ and w_2 as follows:

$$w_0 = \frac{\pi(z)\alpha^2(y^2-a^2)}{2(1+x\delta)}, \quad (23)$$

$$w_1 = \frac{-5 a^4\pi(z)\alpha^4\delta^2 + 6a^2\pi(z)y^2\alpha^4\delta^2 - \pi(z)y^4\alpha^4\delta^2}{24(1+x\delta)^3}, \quad (24)$$

$$w_2 = (\pi(z)(a-y)(a+y)\alpha^4\delta^2(10(-5a^2+y^2) + 20x(-5a^2+y^2)\delta$$
$$+(10x^2(-5a^2+y^2) + 3(61a^4 - 14a^2y^2 + y^4)\alpha^2)\delta^2))$$
$$/240(1+x\delta)^5 \quad (25)$$

According to the rules of HPM, we assume a series solution as given as follows:

$$w(x,y) = \hat{w}(x,y)\big|_{q\to 1} = w_0 + qw_1 + q^2 w_2 + \dots. \quad (26)$$

Now, substituting the values of $w_0, w_1,$ and w_2 into Eq. 26, we obtain the subsequent final solution:

$$w(x,y) = -\frac{1}{80(1+x\delta)^5}(\pi(z)(a-y)(a+y)\alpha^2$$
$$\times(40 + 160x\delta + 240x^2\delta^2\,160x^3\delta^3$$
$$+(40x^4 + (61a^4 - 14a^2y^2 + y^4)\alpha^4)\delta^4)) \quad (27)$$

Here, $\pi(z) = -E_1\phi\cos[t-z] - E_2\phi\cos[t-z] + E_3\phi\cos[t-z]$.

4 Graphical data and discussion

In this section, the manual calculations are converted into graphs of some key parameters, such as axial velocity against the vertical coordinate and axial velocity versus the curvature and trapping bolus to examine the patterns of flow behavior. In Figures 2A–5A, B, the axial velocity function has been presented along the coordinate y axis under a monotonic increase in the absolute values of the aspect ratio (α), mass per unit area E_1, viscous damping force E_2, flexure rigidity
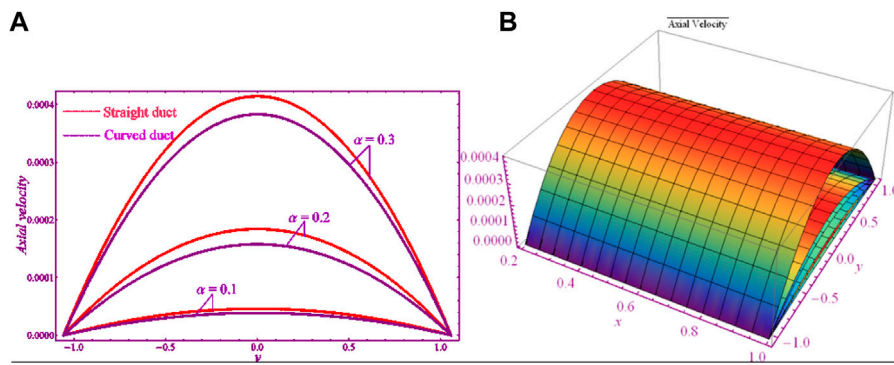
FIGURE 2
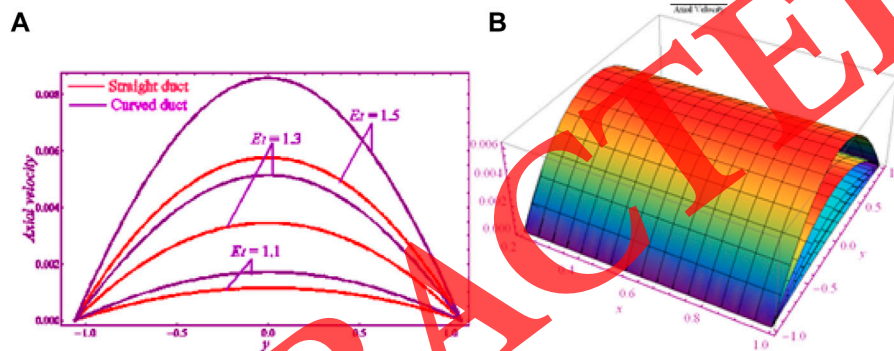Axial velocity profile for the aspect ratio, α. **(A)** 2D. **(B)** 3D.

FIGURE 3
Axial velocity profile for mass per unit area, E_1. **(A)** 2D. **(B)** 3D.
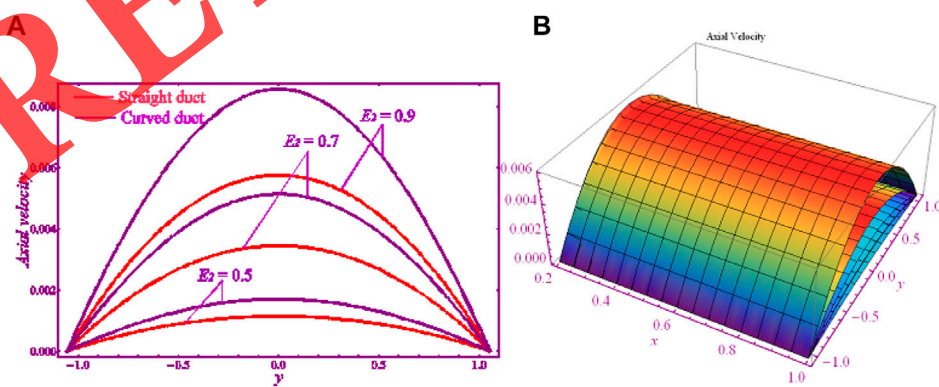

FIGURE 4
Axial velocity profile for viscous damping force, E_2. **(A)** 2D. **(B)** 3D.

E_3, and amplitude ratio ϕ, both in 2-D and 3-D views, accordingly. In each of these graphs, a quantitative comparison is also shown for curved ducts vs straight ducts. All these graphs have been structured for the horizontal range of coordinate y as $[-a, a]$ where

a is the wave height function which directly relates to the angular coordinate $''z''$. Figures 6–9 have been designed to visualize the variation in velocity curvature domain. These figures show the impact of α, E_1, E_2, and ϕ on the profile of velocity w, respectively,
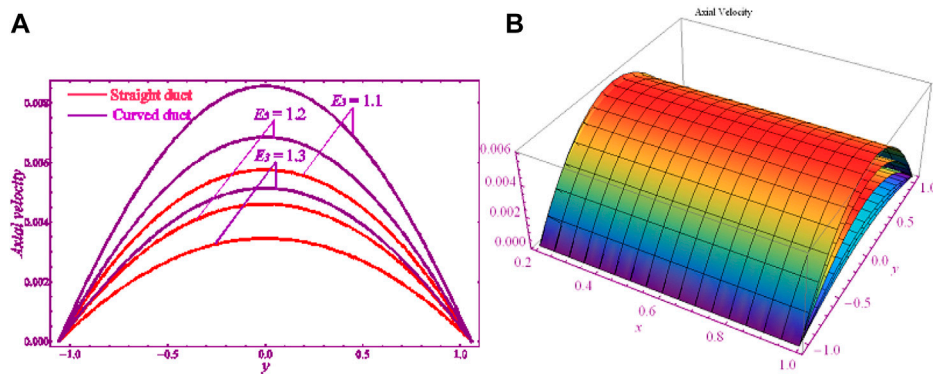
FIGURE 5
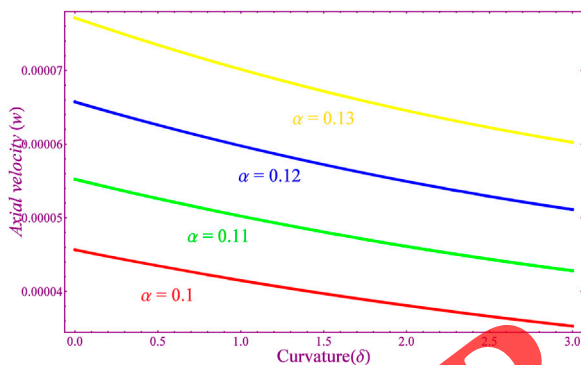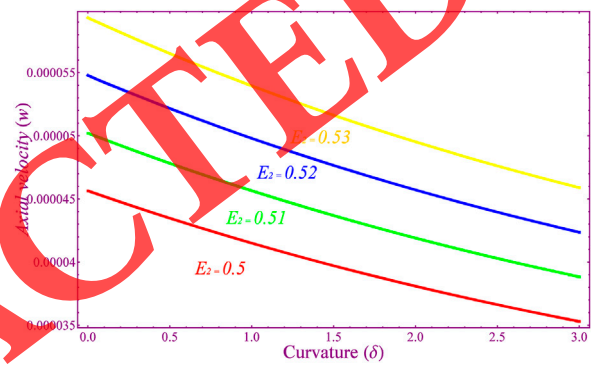Axial velocity profile for flexure rigidity, E_3. **(A)** 2D. **(B)** 3D.

FIGURE 6
w-δ curves for α.

FIGURE 8
w-δ curves for E_2.
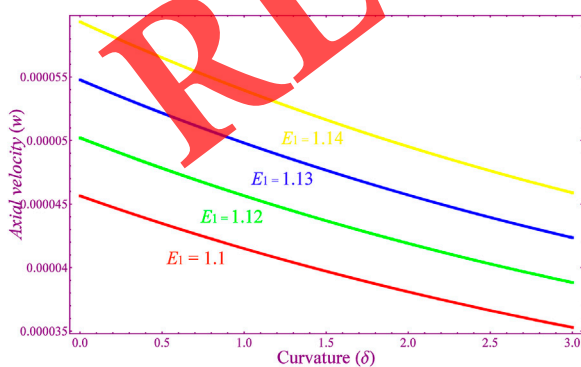
FIGURE 7
w-δ curves for E_1.

FIGURE 9
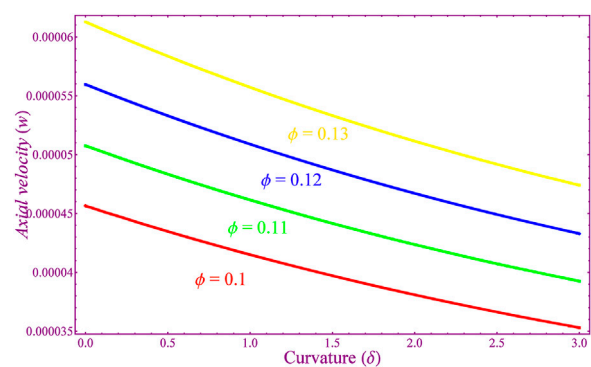w-δ curves for ϕ.

and show how the fluid velocity depends on the overall impact of duct curvature. In these diagrams, a uniform range [0,3] of the parameter δ was taken to investigate the impact of curvature on

flow. Figures 10 and 11 have been included to estimate the quantitative analysis of contourvariations for various emerging parameters like α, and E_1, correspondingly.
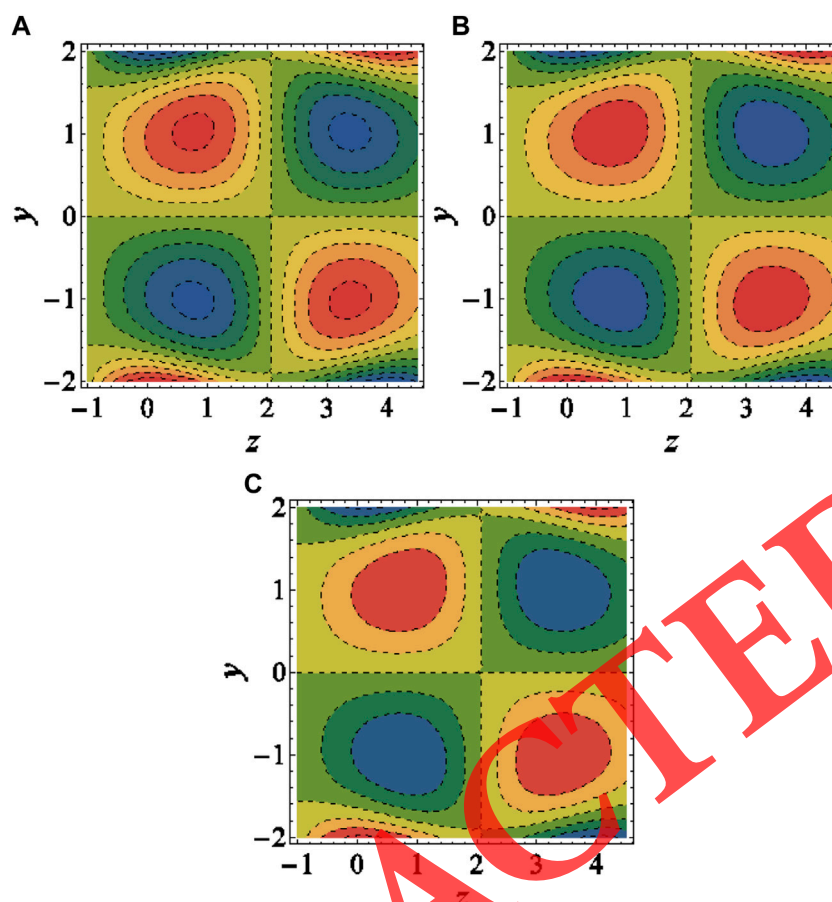
FIGURE 10
(A–C) Flow pattern for α.

Figure 2 shows the graphical behavior of axial velocity for increasing values of the aspect ratio factor α. It can be seen that the fluid velocity is directly affected by the aspect ratio. The aspect ratio is the ratio of width to height of the rectangular cross-section of the duct, so the aspect ratio is increased by increasing the length while keeping the height fixed. Increasing the aspect ratio exerts more pressure on the fluid and pushes it forward faster. It should also be noted here that fluid speed is faster in a straight duct compared to a curved enclosure, possibly due to the turning effects of the walls. Figure 3 shows the velocity variation relative to the mass per unit area E_1. The graph shows that a large mass per unit area causes the fluid to flow at a greater velocity, but in this case, the flow in a straight duct is slower than the flow in a curved duct. The effects of viscous damping force E_2 on the fluid flow can be examined in Figure 4, which shows that velocity becomes larger with increasing damping force in both straight and curved ducts. In contrast, flexure rigidity E_3 has an inverse impact on fluid flow by decreasing its speed (Figure 5). This can be physically explained as the compliance of the rigid walls opposing the flow by applying extra resistance in the direction of the stream. In the three-dimensional graphs, Figures 2–5B, we can see that the velocity remains uniform along the radial direction of the enclosure because of the presence of uniform flow and the absence of boundary slip in most parts of the domain; however, maximum velocity is observed near the central line where $x \approx 0.2$.

To assess the velocity attributes near the domain of curvature, Figure 6 illustrates the impact of α on velocity. From this diagram, it can be seen that when we increase the curvature of the section, the fluid moves at a lower speed, which can be finalized for $\delta = 0$ (straight duct) where there is maximum velocity and for $\delta = 3$ (large curvature) with the lowest velocity. Moreover, the velocity curves are elevated by increasing the aspect ratio. Figure 7 indicates that E_1 has a direct effect on the velocity curves when these are plotted for the curvature domain; however, in this graph, the curves are more parabolic than the previous figure (Figure 6). Figure 8 shows how the curvature affects velocity, when the parametric values of E_2 are varied. According to the calculations, E_2 results in a similar variation, as obtained for E_1. The influence of the amplitude ratio ϕ on the velocity–curvature curves is pictured in Figure 9. The amplitude ratio is linearly related to the velocity but curves downward from the left domain to the right side. Overall, a larger curvature results in a reduction in fluid speed in its axial direction.

Figure 10 shows the trapping bolus mechanism of the flow in relation to the increasing amplitude of the aspect ratio factor α. It can be assumed here that the trapping bolus is extending its dimensions, while the closed contours are reducing its magnitude,
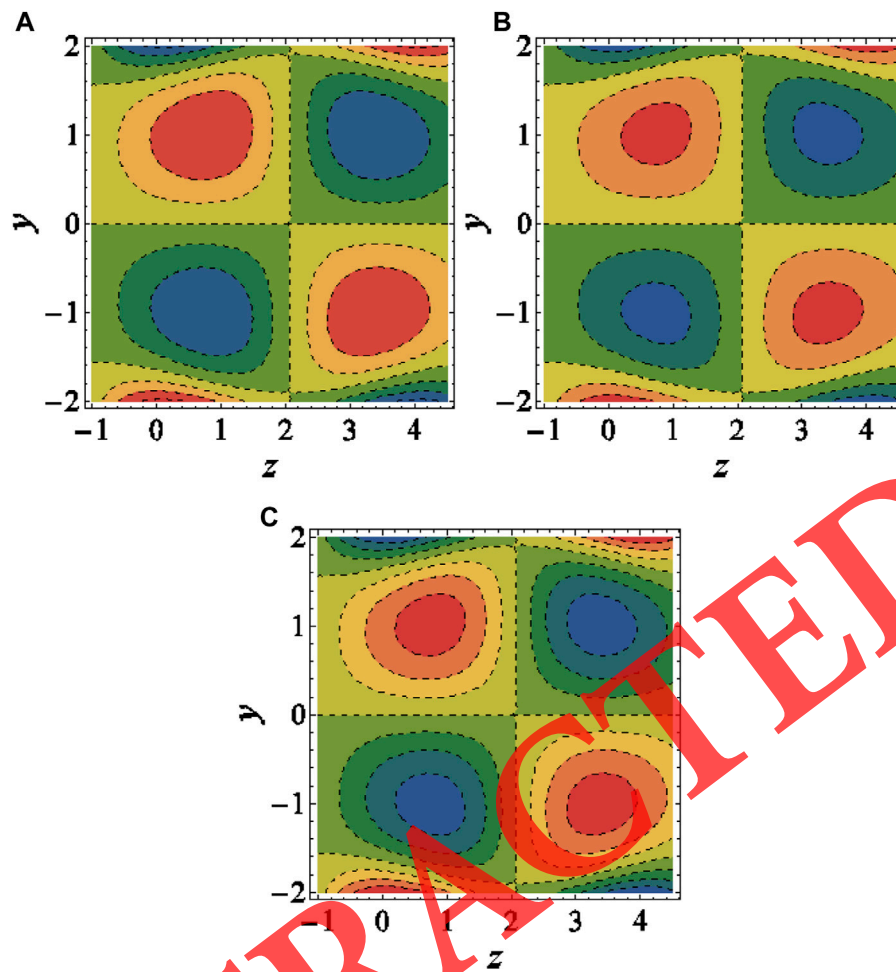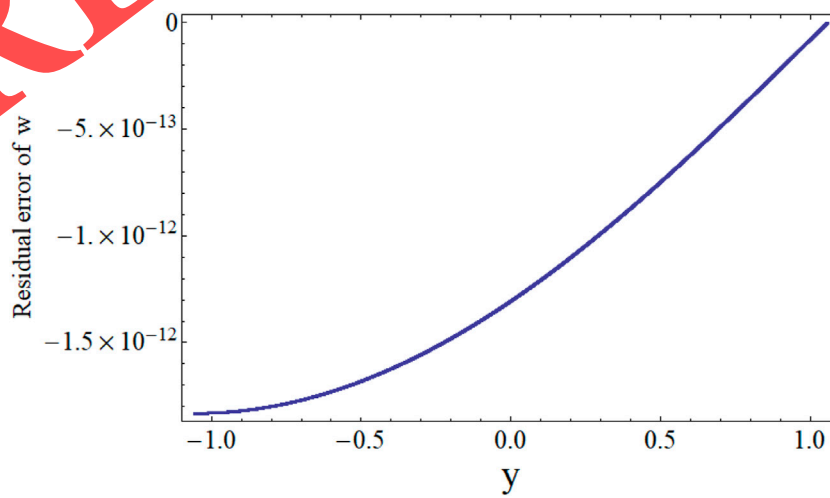
FIGURE 11
(A–C) Flow pattern for E_1.

FIGURE 12
Residual error curve for the axial velocity function, w.

which indicates that more fluid travels through the section when the aspect ratio of the rectangular face is increased. Due to the variation in E_1 of the compliant walls, the boluses are enlarged which shows that fluid can easily pass by the channel by increasing damping force (Figure 11). It should also be noted that there is a symmetric variation in bolus shape across the central line which reveals the physical aspect that compliant walls affect the flow more strongly than the plane region of the geometry. From these results, it is concluded that boluses are highly affected by the curvature of the geometry and that the straight duct readings can be retained by reducing the value of the curvature parameter, δ.

Figure 12 validates the results by collecting residual error data obtained from the solution and the governing differential equations. From the figure, it can be seen that the results are quite satisfactory because the residual error is very small throughout the solution domain. Near the right edge, the error approaches zero which not only ensures that the solution justifies the equation but also satisfies the boundary conditions.

5 Conclusions

In this study, the authors have analyzed the peristaltic flow phenomenon for a viscous fluid in a curved duct having a rectangular cross-section with compliant walls. After incorporating certain limitations, the derivation of the PDEs was achieved by applying the well-known perturbation scheme (HPM) and making use of the computational software application Mathematica through the DSolve tool. Stream functions were obtained using the Integrate tool. The analytical solutions are illustrated in graphs, and the diagrammatical observations were discussed thoroughly. The key findings of this study can be summarized as follows:

1. With the current duct geometry, the velocity was reduced by larger aspect ratios as compared to the straight ducts, but it can be seen that the velocity can also be increased by the larger effect of compliant walls in a curved duct.
2. It was found that velocity is an inverse function of flexural rigidity of the walls, but inverse characteristics have also been reported for the aspect ratio, viscous damping, and mass per unit area.
3. It was found that increasing the curvature of the conduit caused the fluid to travel more slowly.

4. It was observed that compliance of the walls reduced the bolus size but increased the bolus number.
5. More studies on this topic with regard to magnetic fields and slip conditions need to be performed to render these results useful in the field of medical sciences where curved surfaces are encountered for electrically conducting fluids.

Data availability statement

The raw data supporting the conclusion of this article will be made available by the authors, without undue reservation.

Author contributions

All authors listed have made a substantial, direct, and intellectual contribution to the work and approved it for publication.

Acknowledgments

Conflict of interest

The authors declare that the research was conducted in the absence of any commercial or financial relationships that could be construed as a potential conflict of interest.

Publisher's note

All claims expressed in this article are solely those of the authors and do not necessarily represent those of their affiliated organizations, or those of the publisher, the editors, and the reviewers. Any product that may be evaluated in this article, or claim that may be made by its manufacturer, is not guaranteed or endorsed by the publisher.

References

1. Javed M, Naz R. Peristaltic flow of a realistic fluid in a compliant channel. *Physica A: Stat Mech its Appl* (2020) 551:123895. doi:10.1016/j.physa.2019.123895

2. Khan LA, Raza M, Mir NA, Ellahi R. Effects of different shapes of nanoparticles on peristaltic flow of MHD nanofluids filled in an asymmetric channel. *J Therm Anal Calorim* (2020) 140:879–90. doi:10.1007/s10973-019-08348-9

3. Raza M, Ellahi R, Sait SM, Sarafraz MM, Shadloo MS, Waheed I. Enhancement of heat transfer in peristaltic flow in a permeable channel under induced magnetic field using different CNTs. *J Therm Anal Calorim* (2020) 140:1277–91. doi:10.1007/s10973-019-09097-5

4. Imran N, Javed M, Sohail M, Tlili I. Simultaneous effects of heterogeneous-homogeneous reactions in peristaltic flow comprising thermal radiation: Rabinowitsch fluid model. *J Mater Res Technol* (2020) 9(3):3520–9. doi:10.1016/j.jmrt.2020.01.089

5. Hayat T, Zahir H, Mustafa M, Alsaedi A. Peristaltic flow of Sutterby fluid in a vertical channel with radiative heat transfer and compliant walls: A numerical study. *Results Phys* (2016) 6:805–10. doi:10.1016/j.rinp.2016.10.015

6. Akram J, Akbar NS, Tripathi D. Electroosmosis augmented MHD peristaltic transport of SWCNTs suspension in aqueous media. *J Therm Anal Calorim* (2022) 147(3):2509–26. doi:10.1007/s10973-021-10562-3

7. Akbar NS, Maraj EN, Noor NFM, Habib MB. Exact solutions of an unsteady thermal conductive pressure driven peristaltic transport with temperature-dependent nanofluid viscosity. *Case Stud Therm Eng* (2022) 35:102124. doi:10.1016/j.csite.2022.102124

8. Akram J, Akbar NS, Alansari M, Tripathi D. Electroosmotically modulated peristaltic propulsion of TiO2/10W40 nanofluid in curved microchannel. *Int Commun Heat Mass Transfer* (2022) 136:106208. doi:10.1016/j.icheatmasstransfer.2022.106208

9. Bhatti MM, Zeeshan A, Ellahi R, Shit GC. Mathematical modeling of heat and mass transfer effects on MHD peristaltic propulsion of two-phase flow through a Darcy-Brinkman-Forchheimer porous medium. *Adv Powder Technol* (2018) 29(5):1189–97. doi:10.1016/j.apt.2018.02.010

10. Akram J, Akbar NS, Tripathi D. Analysis of electroosmotic flow of silver-water nanofluid regulated by peristalsis using two different approaches for nanofluid. *J Comput Sci* (2022) 62:101696. doi:10.1016/j.jocs.2022.101696

11. Rasool G, Shah NA, El-Zahar ER, Wakif A. Numerical investigation of EMHD nanofluid flows over a convectively heated riga pattern positioned horizontally in a Darcy-forchheimer porous medium: Application of passive control strategy and generalized transfer laws. *Waves in Random and Complex Media* (2022) 1–20. doi:10.1080/17455030.2022.2074571

12. Shah NA, Wakif A, El-Zahar ER, Thumma T, Yook SJ. Heat transfers thermodynamic activity of a second-grade ternary nanofluid flow over a vertical plate with Atangana-Baleanu time-fractional integral. *Alexandria Eng J* (2022) 61(12):10045–53. doi:10.1016/j.aej.2022.03.048

13. Rashid M, Ansar K, Nadeem S. Effects of induced magnetic field for peristaltic flow of Williamson fluid in a curved channel. *Physica A: Stat Mech its Appl* (2020) 553: 123979. doi:10.1016/j.physa.2019.123979

14. Saleem A, Akhtar S, Alharbi FM, Nadeem S, Ghalambaz M, Issakhov A. Physical aspects of peristaltic flow of hybrid nano fluid inside a curved tube having ciliated wall. *Results Phys* (2020) 19:103431. doi:10.1016/j.rinp.2020.103431

15. Riaz A, Khan SUD, Zeeshan A, Hassan M, Muhammad T. Thermal analysis of peristaltic flow of nanosized particles within a curved channel with second-order partial slip and porous medium. *J Therm Anal Calorim* (2021) 143:1997–2009. doi:10.1007/s10973-020-09454-9

16. Ahmed R, Ali N, Khan SU, Tlili I. Numerical simulations for mixed convective hydromagnetic peristaltic flow in a curved channel with joule heating features. *AIP Adv* (2020) 10(7):075303. doi:10.1063/5.0010964

17. Hina S, Hayat T, Alsaedi A. Heat and mass transfer effects on the peristaltic flow of Johnson–Segalman fluid in a curved channel with compliant walls. *Int J Heat Mass Transfer* (2012) 55(13-14):3511–21. doi:10.1016/j.ijheatmasstransfer.2012.03.014

18. Ellahi R, Bhatti MM, Vafai K. Effects of heat and mass transfer on peristaltic flow in a non-uniform rectangular duct. *Int J Heat Mass Transfer* (2014) 71:706–19. doi:10.1016/j.ijheatmasstransfer.2013.12.038

19. Mekheimer KS, Husseny SA, Abd el Lateef AI. Effect of lateral walls on peristaltic flow through an asymmetric rectangular duct. *Appl Bionics Biomech* (2011) 8(34): 295–308. doi:10.1155/2011/424183

20. Akram S, Saleem N. Analysis of heating effects and different wave forms on peristaltic flow of Carreau fluid in rectangular duct. *Adv Math Phys* (2020) 2020:1–14. doi:10.1155/2020/8294318

21. McCash LB, Nadeem S, Akhtar S, Saleem A, Saleem S, Issakhov A. Novel idea about the peristaltic flow of heated Newtonian fluid in elliptic duct having ciliated walls. *Alexandria Eng J* (2021) 61:2697–707. doi:10.1016/j.aej.2021.07.035

22. Akbar NS, Butt AW. Ferromagnetic nano model study for the peristaltic flow in a plumb duct with permeable walls. *Microsystem Tech* (2019) 25(4):1227–34. doi:10.1007/s00542-018-4045-5

23. Rudolf P, Desová M. Flow characteristics of curved ducts. *Appl Comput Mech* (2007) 1(1):255–64.

24. Li Y, Wang X, Yuan S, Tan SK. Flow development in curved rectangular ducts with continuously varying curvature. *Exp Therm Fluid Sci* (2016) 75:1–15. doi:10.1016/j.expthermflusci.2016.01.012

25. Ghia KN, Sokhey JS, 1977. *Laminar incompressible viscous flow in curved ducts of regular cross-sections*.

26. Dolon SN, Hasan MS, Lorenzini G, Mondal RN. A computational modeling on transient heat and fluid flow through a curved duct of large aspect ratio with centrifugal instability. *The Eur Phys J Plus* (2021) 136(4):382–27. doi:10.1140/epjp/s13360-021-01331-0

27. Riaz A, Ahammad NA, Alqarni MM, Hejazi HA, Tag-ElDin EM. Peristaltic flow of a viscous fluid in a curved duct with a rectangular cross section. *Front Phys* (2022) 666. doi:10.3389/fphy.2022.961201

28. Kumar MD, Raju CSK, Sajjan K, El-Zahar ER, Shah NA. Linear and quadratic convection on 3D flow with transpiration and hybrid nanoparticles. *Int Commun Heat Mass Transfer* (2022) 134:105995. doi:10.1016/j.icheatmasstransfer.2022.105995

29. Sajjan K, Shah NA, Ahammad NA, Raju CSK, Kumar MD, Weera W, et al. Nonlinear Boussinesq and Rosseland approximations on 3D flow in an interruption of Ternary nanoparticles with various shapes of densities and conductivity properties. *AIMS Math* (2022) 7(10):18416–49. doi:10.3934/math.20221014

30. Biazar J, Ghazvini H. Homotopy perturbation method for solving hyperbolic partial differential equations. *Comput Maths Appl* (2008) 56(2):453–8. doi:10.1016/j.camwa.2007.10.032

31. Mohyud-Din ST, Noor MA. Homotopy perturbation method for solving partial differential equations. *Z für Naturforschung A* (2009) 64(3-4):157–70. doi:10.1515/zna-2009-3-402

32. Dehghan M, Shakeri F. Use of He's homotopy perturbation method for solving a partial differential equation arising in modeling of flow in porous media. *J Porous Media* (2008) 11(8):765–78. doi:10.1615/jpormedia.v11.i8.50

Nomenclature

Symbols definition

h height

d width

c wave speed

t time coordinate

$(u, v, \text{ and } w)$ velocity components

ρ density

μ viscosity

$\tilde{a}$ wave function

b amplitude

λ wavelength

L length

p pressure

$\boldsymbol{\tau}$ elastic membrane tension

σ mass over unit area

ε viscous damping coefficient

dimensionless symbols

$\bar{t}, \bar{x}, \bar{y}, \text{ and } \bar{z}$ dimensionless independent coordinates

$(r, \theta, \text{ and } y)$ curvilinear cylindrical coordinates

$(x, y, \text{ and } z)$ transformed coordinates

$\bar{p}$ dimensionless pressure

$(u, v, \text{ and } w)$ dimensionless velocity components

$\bar{a}$ dimensionless wave function

ξ dimensionless wave number

α aspect ratio

δ dimensionless curvature

Re Reynolds number

ϕ amplitude ratio

$E_1, E_2, \text{ and } E_3$ compliant wall parameters